JOURNAL OF VIROLOGY, July 2009, p. 7322–7336 Vol. 83, No. 14
0022-538X/09/$08.00+0 doi:10.1128/JVI.02545-08

Quantitative Fluorescence Resonance Energy Transfer Microscopy Analysis of the Human Immunodeficiency Virus Type 1 Gag-Gag Interaction: Relative Contributions of the CA and NC Domains and Membrane Binding▽†

Ian B. Hogue,[1] Adam Hoppe,[1,2]‡ and Akira Ono[1]*

Department of Microbiology and Immunology,[1] and Center for Live-Cell Imaging,[2] University of Michigan Medical School, Ann Arbor, Michigan 48109

Received 10 December 2008/Accepted 21 April 2009

The human immunodeficiency virus type 1 structural polyprotein Pr55^{Gag} is necessary and sufficient for the assembly of virus-like particles on cellular membranes. Previous studies demonstrated the importance of the capsid C-terminal domain (CA-CTD), nucleocapsid (NC), and membrane association in Gag-Gag interactions, but the relationships between these factors remain unclear. In this study, we systematically altered the CA-CTD, NC, and the ability to bind membrane to determine the relative contributions of, and interplay between, these factors. To directly measure Gag-Gag interactions, we utilized chimeric Gag-fluorescent protein fusion constructs and a fluorescence resonance energy transfer (FRET) stoichiometry method. We found that the CA-CTD is essential for Gag-Gag interactions at the plasma membrane, as the disruption of the CA-CTD has severe impacts on FRET. Data from experiments in which wild-type (WT) and CA-CTD mutant Gag molecules are coexpressed support the idea that the CA-CTD dimerization interface consists of two reciprocal interactions. Mutations in NC have less-severe impacts on FRET between normally myristoylated Gag proteins than do CA-CTD mutations. Notably, when nonmyristoylated Gag interacts with WT Gag, NC is essential for FRET despite the presence of the CA-CTD. In contrast, constitutively enhanced membrane binding eliminates the need for NC to produce a WT level of FRET. These results from cell-based experiments suggest a model in which both membrane binding and NC-RNA interactions serve similar scaffolding functions so that one can functionally compensate for a defect in the other.

The human immunodeficiency virus type 1 (HIV-1) structural precursor polyprotein Pr55^{Gag} is necessary and sufficient for the assembly of virus-like particles (VLPs). Gag is composed of four major structural domains, matrix (MA), capsid (CA), nucleocapsid (NC), and p6, as well as two spacer peptides, SP1 and SP2 (3, 30, 94). Following particle assembly and release, cleavage by HIV-1 protease separates these domains. However, these domains must work together in the context of the full-length Gag polyprotein to drive particle assembly.

Previous studies have mapped two major functional domains involved in the early steps of assembly: first, Gag associates with cellular membranes via basic residues and N-terminal myristoylation of the MA domain (10, 17, 20, 35, 39, 87, 91, 106); second, the Gag-Gag interaction domains that span the CA C-terminal domain (CA-CTD) and NC domain promote Gag multimerization (3, 11, 14, 16, 18, 23, 27, 29, 30, 33, 36, 46, 64, 88, 94, 102, 103). Structural and genetic studies have identified two residues (W184 and M185) within a dimerization interface in the CA-CTD that are critical to CA-CA interactions (33, 51, 74, 96). Analytical ultracentrifugation of heterodimers formed between wild-type (WT) Gag and Gag mutants with changes at these residues suggests that the dimerization interface consists of two reciprocal interactions, one of which can be disrupted to form a "half-interface" (22).

In addition to the CA-CTD, NC contributes to assembly via 15 basic residues (8, 9, 11, 14, 18, 23, 25, 28, 34, 40, 43, 54, 57, 58, 74, 79, 88, 97, 104, 105), although some researchers have suggested that NC instead contributes to the stability of mature virions after assembly (75, 98, 99). It is thought that the contribution of NC to assembly is due to its ability to bind RNA, since the addition of RNA promotes the formation of particles in vitro (14–16, 37, 46), and RNase treatment disrupts Gag-Gag interactions (11) and immature viral cores (67). However, RNA is not necessary per se, since dimerization motifs can substitute for NC (1, 4, 19, 49, 105). This suggests a model in which RNA serves a structural role, such as a scaffold, to promote Gag-Gag interactions through NC. Based on in vitro studies, it has been suggested that this RNA scaffolding interaction facilitates the low-order Gag multimerization mediated by CA-CTD dimerization (4, 37, 49, 62, 63, 85). Despite a wealth of biochemical data, the relative contributions of the CA-CTD and NC to Gag multimerization leading to assembly are yet to be determined in cells.

Mutations in Gag interaction domains alter membrane binding in addition to affecting Gag multimerization. In particular, mutations or truncations of CA reduce membrane binding (21,

* Corresponding author. Mailing address: Department of Microbiology and Immunology, University of Michigan Medical School, 5736 Medical Science Bldg. II, 1150 W. Medical Center, Dr. Ann Arbor, MI 48109. Phone: (734) 615-4407. Fax: (734) 746-3562. E-mail: akiraono@umich.edu.

† Supplemental material for this article may be found at http://jvi.asm.org/.

‡ Present address: Department of Chemistry and Biochemistry, South Dakota State University, Brookings, SD 57007.

▽ Published ahead of print on 29 April 2009.

74, 82), and others previously reported that mutations or truncations of NC affect membrane binding (13, 78, 89, 107). These findings are consistent with a myristoyl switch model of membrane binding in which Gag can switch between high- and low-membrane-affinity states (38, 71, 76, 83, 86, 87, 92, 95, 107). Many have proposed, and some have provided direct evidence (95), that Gag multimerization mediated by CA or NC interactions promotes the exposure of the myristoyl moiety to facilitate membrane associations.

Gag membrane binding and multimerization appear to be interrelated steps of virus assembly, since membrane binding also facilitates Gag multimerization. Unlike betaretroviruses that fully assemble prior to membrane targeting and envelopment (type B/D), lentiviruses, such as HIV, assemble only on cellular membranes at normal Gag expression levels (type C), although non-membrane-bound Gag complexes exist (45, 58, 60, 61, 65). Consistent with this finding, mutations that reduce Gag membrane associations cause a defect in Gag multimerization (59, 74). Therefore, in addition to their primary effects on Gag-Gag interactions, mutations in Gag interaction domains cause a defect in membrane binding, which, in turn, causes a secondary multimerization defect. To determine the relative contributions of the CA-CTD and the NC domain to Gag-Gag interactions at the plasma membrane, it is essential to eliminate secondary effects due to a modulation of membrane binding.

Except for studies using a His-tag-mediated membrane binding system (5, 46), biochemical studies of C-type Gag multimerization typically lack membranes. Therefore, these studies do not fully represent particle assembly, which occurs on biological membranes in cells. Furthermore, many biochemical and structural approaches are limited to isolated domains or truncated Gag constructs. Thus, some of these studies are perhaps more relevant to the behavior of protease-cleaved Gag in mature virions. With few exceptions (47, 74), cell-based studies of Gag multimerization have typically been limited to measuring how well mutant Gag is incorporated into VLPs when coexpressed or not with WT Gag. Since VLP production is a complex multistep process, effects of mutations on other steps in the process can confound this indirect measure. For example, NC contributes to VLP production by both promoting multimerization and interacting with the host factor ALIX to promote VLP release (26, 80). To directly assay Gag multimerization in cells, several groups (24, 45, 52, 56) developed microscopy assays based on fluorescence resonance energy transfer (FRET). These assays measure the transfer of energy between donor and acceptor fluorescent molecules that are brought within ~5 nm by the association of the proteins to which they are attached (41, 48, 90). However, these microscopy-based Gag FRET assays have not been used to fully elucidate several fundamental aspects of HIV-1 Gag multimerization at the plasma membrane of cells, such as the relative contributions of the CA-CTD and NC and the effect of membrane binding on Gag-Gag interactions. In this study, we used a FRET stoichiometry method based on calibrated spectral analysis of fluorescence microscopy images (41). This algorithm determines the fractions of both donor and acceptor fluorescent protein-tagged Gag molecules participating in FRET. For cells expressing Gag molecules tagged with donor (cyan fluorescent protein [CFP]) and acceptor (yellow fluorescent protein [YFP]) molecules, this method measures the apparent FRET efficiency, which is proportional to the mole fraction of Gag constructs in complex. By measuring apparent FRET efficiencies, quantitative estimates of the mole fractions of interacting proteins can be obtained.

Using this FRET-based assay, we aim to answer two questions: (i) what are the relative contributions of CA-CTD and NC domains to Gag multimerization when secondary effects via membrane binding are held constant, and (ii) what is the effect of modulating membrane binding on the ability of Gag mutants to interact with WT Gag?

Our data demonstrate that the CA-CTD dimerization interface is essential for Gag multimerization at the plasma membrane, as fully disrupting the CA-CTD interaction abolishes FRET, whereas a modest level of FRET is still detected in the absence of NC. We also present evidence that the CA-CTD dimerization interface consists of two reciprocal interactions, allowing the formation of a half-interface that can still contribute to Gag multimerization. Notably, when Gag derivatives with an intact CA-CTD were coexpressed with WT Gag, either membrane binding ability or NC was required for the Gag mutants to interact with WT Gag, suggesting functional compensation between these factors.

MATERIALS AND METHODS

Plasmids. The HIV-1 molecular clone pNL4-3 was described previously (2). The molecular clone encoding nonfunctional viral protease, pNL4-3/PR−, was described previously (44). The derivative pNL4-3/Gag-Venus, encoding Gag with a C-terminal mVenus-variant YFP fusion, was described previously (17). This construct contains an extensive deletion of *pol* and silent mutations to reduce ribosomal frameshift to the *pol* reading frame (17). This construct also does not express *vif* or *vpr* (93). The derivative pNL4-3/Gag-mCerulean, encoding Gag with a C-terminal mCerulean (84) CFP fusion, was generated by replacing mVenus of pNL4-3/Gag-Venus with mCerulean, PCR amplified from pmCerulean-N1 (obtained from S. Straight, University of Michigan Center for Live-Cell Imaging). Plasmid pNL4-3/CA152xba220 was generated by PCR mutagenesis. The sequence coding for residues I153 through Q219 was replaced with an XbaI restriction site, coding for the dipeptide SR. This mutant will be referred to as delCA-CTD for simplicity. The derivative pNL4-3/WM184,185AA was described previously (74). The derivative pNL4-3/14A1G was generated by PCR mutagenesis. The amino acid substitutions were previously described for the 15A NC mutant (18, 79) except that residue R405 was mutated to Gly instead of Ala to preserve the ApaI restriction site, and mutagenesis was performed in a pNL4-3 genetic background. pNL4-3/delNC was a kind gift from D. Ott (75). Chimeric Gag constructs derived from pNL4-3/delNC do not contain silent mutations to reduce ribosomal frameshift to the *pol* reading frame but do retain an extensive deletion of *pol*. pNL4-3/1GA was described previously (32). The construct with the first 10 residues of Fyn kinase replacing the Gag start codon [pNL4-3/Fyn(10)fullMA/GagVenus] was described previously (17). The Gag derivatives used in FRET experiments (Fig. 1) were constructed from the above-mentioned plasmids using standard molecular biology techniques. The mVenus expression plasmid pmVenus-N1 was created by replacing mCerulean in pmCerulean-N1 with mVenus from pNL4-3/Gag-Venus. pFyn(10)-mVenus, which expresses mVenus with an N-terminal 10-residue Fyn kinase acylation signal, was created by PCR mutagenesis. pmCerulean-mVenus-linked was created by replacing mCitrine in pmCerulean-mCitrine (a gift from S. Straight, University of Michigan Center for Live-Cell Imaging) with mVenus from pNL4-3/Gag-Venus. This construct expresses mCerulean and mVenus in tandem, separated by a 27-amino-acid linker encoded by the pmCerulean-N1 multiple-cloning site.

Cells and transfection. HeLa cells were cultured as described previously (31). For microscopy, 4.2×10^4 cells were seeded into each well of eight-well chamber slides (Nalge Nunc, Rochester, NY), grown for 24 h, and transfected with Lipofectamine 2000 (Invitrogen) according to the manufacturer's instructions. For the VLP release assay, membrane flotation, the myristoylation assay, and immunoblotting, 5.6×10^5 cells were seeded into each well of six-well plates (Corning), grown overnight, and transfected as described above.

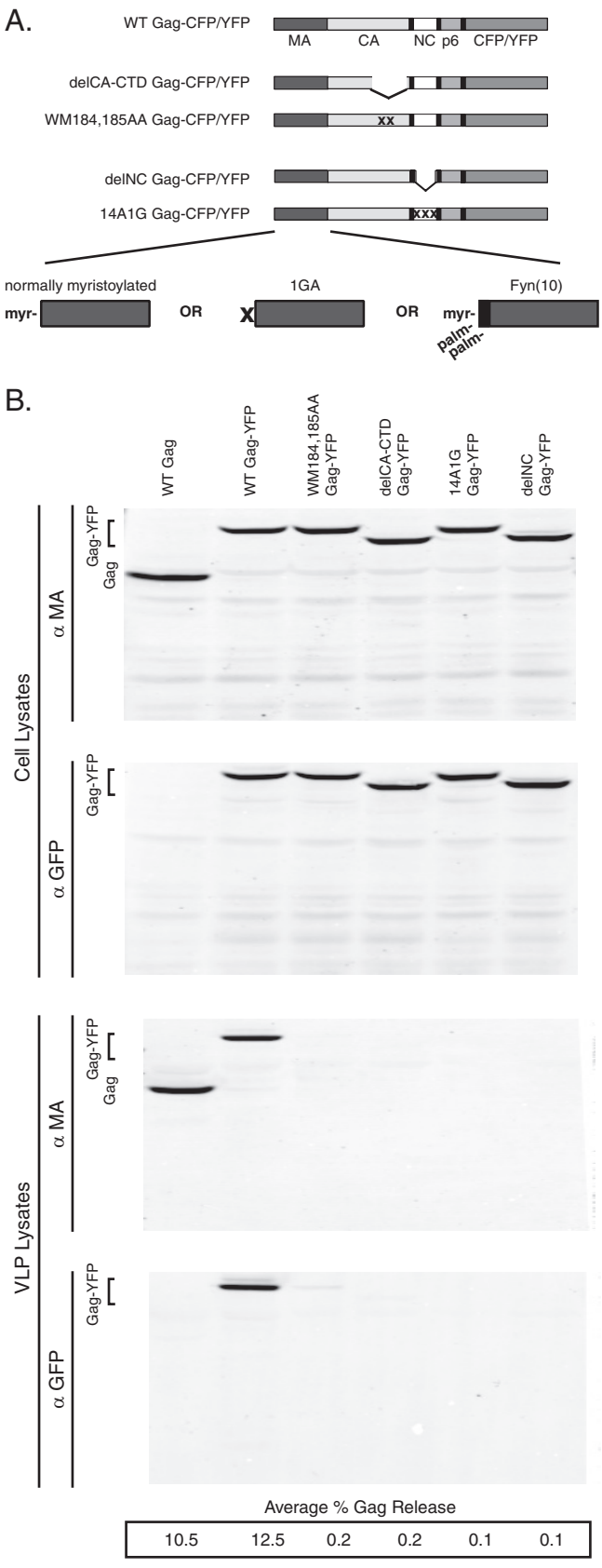

FIG. 1. (A) Gag derivatives used in this study. HIV-1 molecular clones that express chimeric Gag-fluorescent protein fusions (WT Gag-CFP/YFP) were generated. Deletions or amino acid substitutions were created in the CA domain (delCA-CTD and WM184,185AA, respectively) and the NC domain (delNC and 14A1G, respectively). This panel of mutants was additionally altered to reduce membrane binding by abolishing N-terminal myristoylation (1GA) or enhance membrane binding by adding a triple-acylation signal [Fyn(10)]. Sites of N-terminal myristoylation (myr) and palmitoylation (palm) are indicated. (B) Expression and VLP release. VLP release of chimeric Gag-YFP and mutant constructs was compared to that of nonchimeric Gag. Immunoblots were probed to detect the matrix domain of Gag (anti-MA antibody [αMA]) or the YFP tag (anti-GFP antibody [αGFP]) to ensure that chimeric Gag proteins are full length. Data are representative of data from four independent experiments.

VLP release assay. Transfected HeLa cells and supernatants were harvested at 18 h posttransfection. VLPs were pelleted by ultracentrifugation from 0.45-μm-filtered cell supernatants, as previously described (69). Gag constructs in cell lysates and VLPs were detected by immunoblotting using rabbit anti-p17 (Paul Spearman, AIDS Research and Reference Reagent Program, Division of AIDS, NIAID, NIH) and rabbit polyclonal anti-green fluorescent protein (GFP) (Clontech) as primary antibodies and Alexa Fluor 594-conjugated anti-rabbit immunoglobulin G (IgG) as a secondary antibody (Invitrogen). Secondary-antibody fluorescence was quantified using a Typhoon Trio imager (GE Healthcare). VLP release efficiency was calculated as previously described (69).

Membrane flotation assay. Transfected HeLa cells were harvested at 18 to 20 h posttransfection. Cells were prepared for membrane flotation centrifugation as previously described (71). To measure steady-state membrane associations, Gag constructs were detected by immunoblotting as described previously (70). Gag constructs were detected using rabbit polyclonal anti-GFP (Clontech) and Alexa Fluor 488-conjugated anti-rabbit IgG as a secondary antibody (Invitrogen). The amount of Gag in each fraction was quantified using a Typhoon Trio imager (GE Healthcare), and percent membrane binding was calculated by the sum of Gag in membrane fractions 1 and 2 divided by the sum total Gag in all five fractions.

Myristoylation assay. Six hours posttransfection, HeLa cells were metabolically radiolabeled overnight with [^{3}H]myristic acid (Perkin-Elmer) as previously described (71). Chimeric Gag proteins were immunoprecipitated from cell lysates using HIV-Ig (NABI and NHLBI, AIDS Research and Reference Reagent Program, Division of AIDS, NIAID, NIH). Autoradiography was performed as previously described (71). Total Gag protein was detected by immunoblotting using rabbit polyclonal anti-GFP, as described above.

Fluorescence microscopy. At 17 h posttransfection, HeLa cells were rinsed once with phosphate-buffered saline (PBS), fixed in 4% paraformaldehyde (EMS, Hatfield, PA) in PBS for 30 min, rinsed once with PBS, and mounted in Fluoromount-G (Southern Biotech) for two-dimensional (2D) microscopy. Alternatively, for three-dimensional (3D) microscopy, cells were incubated with anti-human CD81 (BD Pharmingen) for 15 min at 37°C without membrane permeabilization to label only cell surface CD81 proteins. Cells were fixed in 4% paraformaldehyde in PBS for 30 min, and the remaining paraformaldehyde was neutralized by adding 0.1 M glycine in PBS. Cells were then blocked with 3% bovine serum albumin in PBS and incubated with Alexa Fluor 594-conjugated anti-mouse IgG as a secondary antibody (Invitrogen). Cells were then imaged immersed in PBS. All microscopy was performed at the University of Michigan Center for Live-Cell Imaging. 2D microscopy was performed using an Olympus (Center Valley, PA) IX70 inverted microscope, with an X-Cite 120 metal halide light source (Exfo, Mississauga, ON, Canada), a 100× (oil immersion UPlan Fl with a numerical aperture of 1.30) objective, a CFP/YFP/red fluorescent protein-optimized filter set (catalog number 86006-SPR; Chroma Technology Corp., Rockingham, VT) mounted in a Lambda 10-3 automatic filter wheel (Sutter Instrument Co., Novato, CA), and a CoolSNAP HQ2 14-bit charge-coupled-device camera (Photometrics, Tucson, AZ) controlled by Metamorph Premier v6.3 software (Molecular Devices, Downingtown, PA). 3D microscopy was performed using a previously described custom-built fluorescence microscope (42). Images were collected using three filter combinations: YFP excitation/YFP emission, CFP excitation/CFP emission, and CFP excitation/YFP emission.

Image analysis, quantitation, and statistics. FRET was calculated from 2D epifluorescence microscopy images using the method of FRET stoichiometry (41). FRET produces two changes in fluorescence signals: (i) a decrease in donor fluorescence and (ii) a proportional increase in acceptor fluorescence. The loss in donor fluorescence due to FRET can be measured by photobleaching the

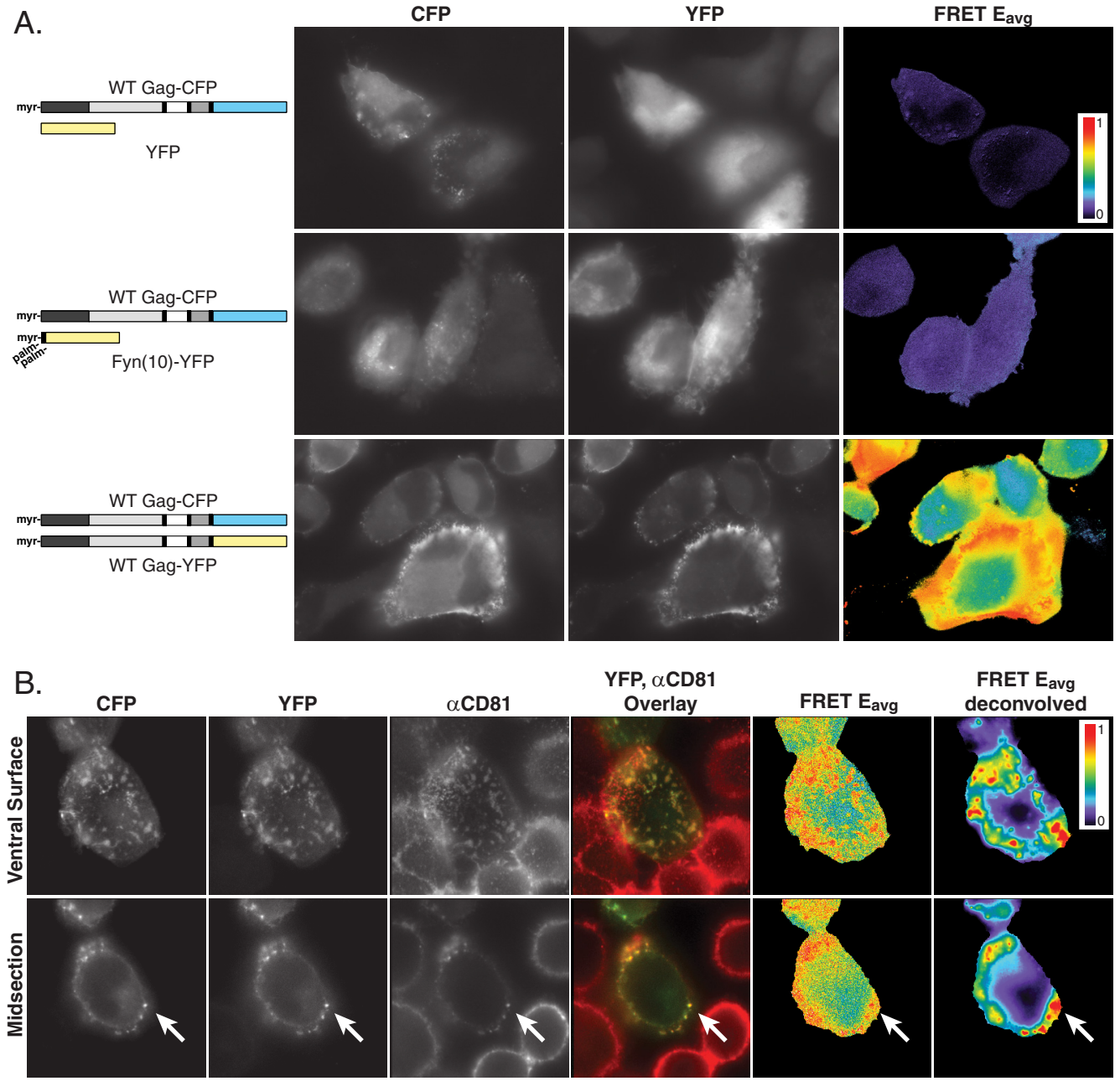

FIG. 2. (A) Stoichiometric FRET microscopy of control and WT Gag constructs. Negative control constructs, YFP (not fused to Gag or any other membrane association signal) and Fyn(10)-YFP (fused to a triple-acylation signal), were coexpressed with WT Gag-CFP. Note that Fyn(10)-YFP fluorescence intensity appears uneven or punctate, which is likely due to the presence of membrane ruffles and blebs. As a positive control, WT Gag-CFP and -YFP were coexpressed. FRET E_{avg} values were calculated from images taken with three filter combinations: CFP excitation/CFP emission (CFP), YFP excitation/YFP emission (YFP), and CFP excitation/YFP emission (not shown). FRET E_{avg} values are color coded according to the scale bar at the top right. (B) Gag FRET is associated predominantly with plasma membrane puncta. WT Gag-CFP/YFP was coexpressed, and cells were immunostained without membrane permeabilization to detect cell surface CD81. Images of WT Gag-YFP (green) and anti-CD81 (αCD81) (red) were overlaid to illustrate colocalization (yellow). FRET E_{avg} values were calculated as described above or with the deconvolution of the 3D image to reduce the contribution of out-of-focus light from other focal planes. myr, myristoylation; palm, palmitoylation.

acceptor and recording the recovery of donor fluorescence. However, these measurements observe only the amount of donor bound by acceptor, which can be influenced by the local ratio of acceptor- and donor-tagged Gag molecules. For example, during heterotypic expression of mutant Gag-YFP and WT Gag-CFP, a minority of mutant Gag-YFP molecules is recruited into a multimer containing a majority of WT Gag-CFP, producing locally skewed ratios of molecules. The use of a FRET method that measures only the degree to which WT Gag-CFP is participating in FRET would produce low FRET efficiency simply because WT Gag-CFP is locally in excess, masking any mutant/WT interaction that may be present.

To overcome this limitation, the FRET stoichiometry algorithm used in this study converts the fluorescence signals from direct donor fluorescence, direct acceptor fluorescence, and acceptor fluorescence due to FRET into measures of molecule concentration and FRET efficiency (41). FRET in this study is reported

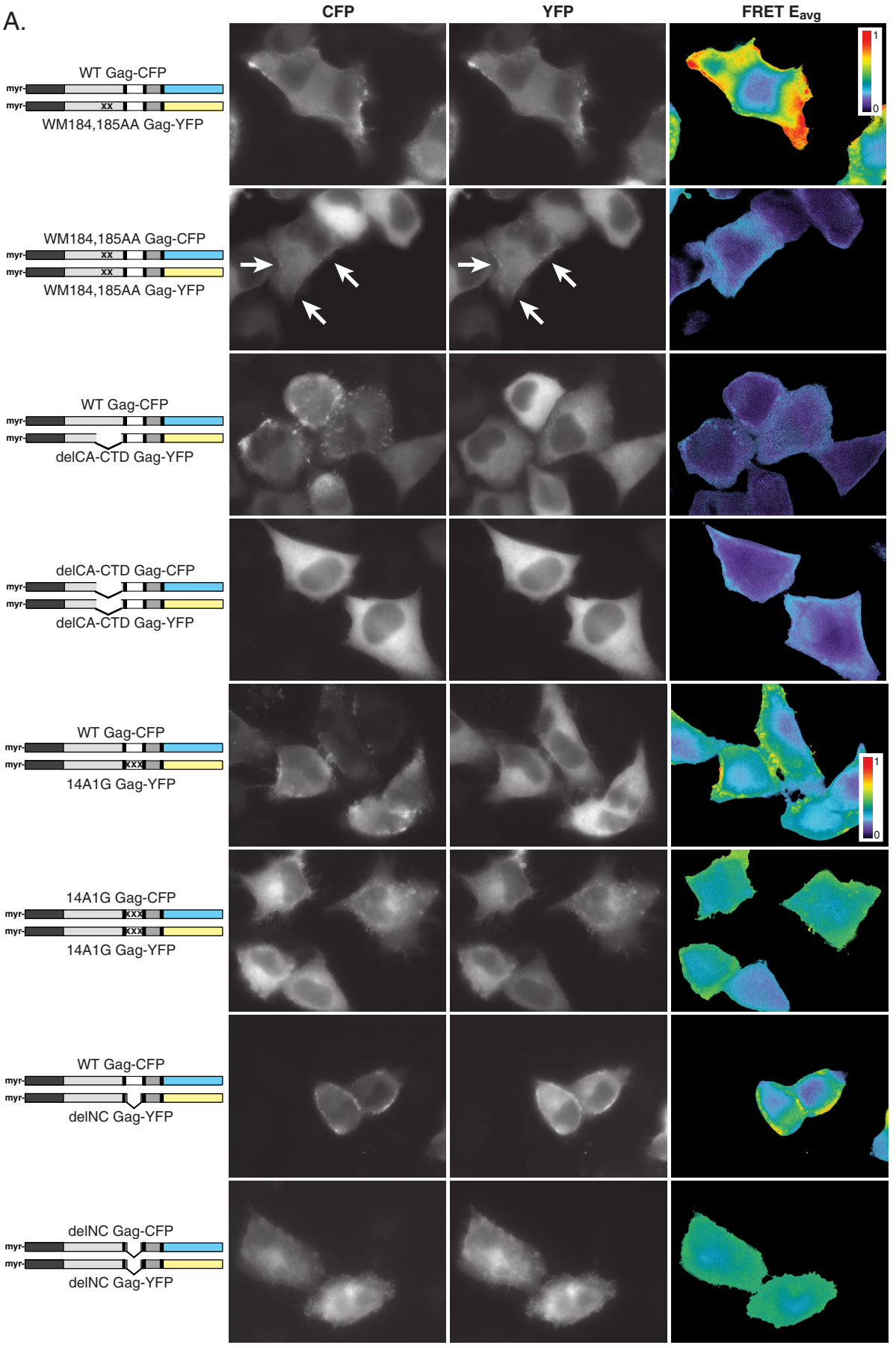
A.
CFP
YFP
FRET E avg
1
0
WT Gag-CFP
myr-
myr-
xx
WM184,185AA Gag-YFP
WM184,185AA Gag-CFP
WM184,185AA Gag-YFP
WT Gag-CFP
delCA-CTD Gag-YFP
delCA-CTD Gag-CFP
delCA-CTD Gag-YFP
WT Gag-CFP
xxx
14A1G Gag-YFP
14A1G Gag-CFP
14A1G Gag-YFP
WT Gag-CFP
delNC Gag-YFP
delNC Gag-CFP
delNC Gag-YFP

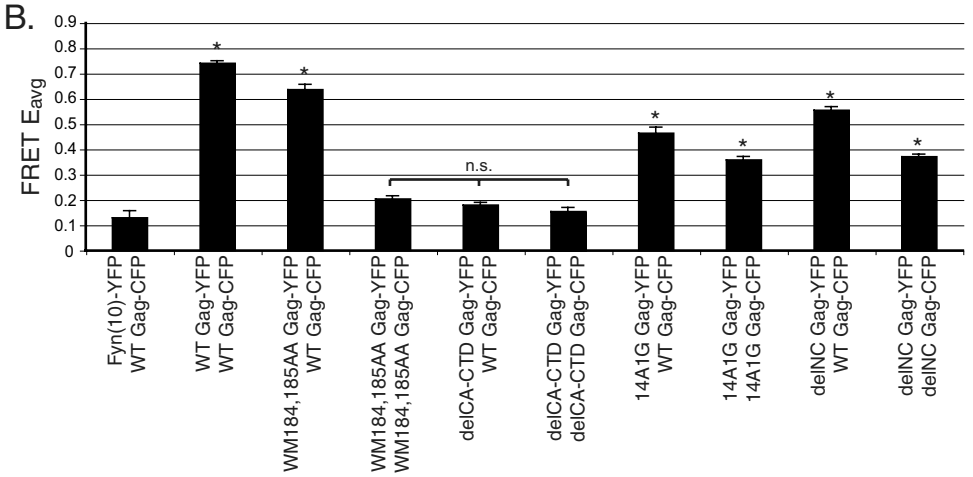

FIG. 3. Stoichiometric FRET microscopy of mutant Gag constructs. (A) Gag-CFP/YFP constructs containing CA mutations (WM184,185AA or delCA-CTD) or NC mutations (14A1G or delNC) were coexpressed homotypically (i.e., both Gag-CFP and Gag-YFP constructs contain the same mutation) or heterotypically (i.e., the Gag-YFP construct contains a mutation, but the Gag-CFP construct does not). FRET E_{avg} values were calculated from images taken with three filter combinations: CFP excitation/CFP emission (CFP), YFP excitation/YFP emission (YFP), and CFP excitation/YFP emission (not shown). FRET E_{avg} values are color coded according to the scale bar at the top right. In the case of WM184,185AA Gag-CFP/YFP homotypic expression, plasma membrane puncta are indicated (arrows). (B) E_{avg} values for fluorescent puncta were quantified over approximately 50 cells (see Fig. S1 in the supplemental material for examples of how regions of interest were selected around fluorescent puncta). Similar results were obtained in more than four independent experiments. *, statistically greater than the Fyn(10)-YFP negative control ($P < 0.01$); n.s., no statistical difference ($P > 0.01$). Error bars represent standard errors of the means. myr, myristoylation.

as average apparent FRET efficiency (E_{avg}), which is proportional to the average mole fraction of fluorophores participating in FRET [$E_{avg} = (E_A + E_D)/2$] according to the nomenclature described previously by Hoppe et al. (41). The E_{avg} value ranges from 0 to 1 and provides a measure of the strength of an interaction with reduced dependence on the relative expression of the donor- and acceptor-tagged molecules (6, 12). Additionally, FRET stoichiometry provides information on the mole fraction of both CFP- and YFP-tagged Gag molecules participating in FRET, providing a more complete measure of Gag-Gag interactions.

For 3D epifluorescence microscopy, FRET was either calculated from single *xy* planes as for 2D microscopy or calculated using a method that reconstructs the 3D distribution of fluorescent molecules by deconvolution (42). These calculations were performed using custom FRET calculator software, implemented using MATLAB (R2008a; The Mathworks, Natick, MA) and developed by the University of Michigan Center for Live-Cell Imaging (available for download at http://sitemaker.umich.edu/4dimagingcenter/).

To calculate FRET stoichiometry, it is necessary to experimentally determine the constants α, β, γ, and ξ. The constants α and β describe the cross talk of donor and acceptor fluorophores into each other's detection channel. The constant γ is the ratio of the extinction coefficients of the two fluorophores, which is necessary to calculate the degree of acceptor fluorophore participation in FRET from the measured increase in acceptor fluorescence due to FRET. The constant ξ relates the increase in acceptor fluorescence due to FRET to the decrease in donor fluorescence due to FRET, which is necessary to calculate the degree of donor fluorophore participation in FRET (41). To experimentally determine the constants α, β, γ, and ξ, HeLa cells were transfected with pmCerulean-N1, pmVenus-N1, or pmCerulean-mVenus-linked. Cells were fixed and mounted, and images were collected as described above. Regions that were positive for fluorescence were manually selected, surrounding approximately 40 fluorescent cells distributed over 10 microscopy fields. The constants α, β, γ, and ξ were calculated from these data as previously described (41).

After calculating FRET E_{avg} values for entire microscopy fields using the FRET stoichiometry method (described above), regions of interest were automatically selected around fluorescent puncta using the GranFilter plugin (81) in ImageJ (version 1.40g; NIH, Bethesda, MD [http://rsb.info.nih.gov/ij/]). Plugin settings were as follows: circular structure element, 5-pixel radius, 1-pixel step size, and image unmasked. With these settings, the GranFilter plugin serves as an image filter to identify regions of interest around fluorescent puncta in a consistent and reproducible manner. FRET E_{avg} values were then recorded at the regions of interest (see Fig. S1 in the supplemental material for GranFilter examples). When multiple regions of interest were measured per cell, measurements were averaged on a cell-by-cell basis so that cells with more puncta identified by GranFilter were not overrepresented in the population statistics. Approximately 40 to 50 cells were measured for each experimental condition. Statistical significance was assessed by a two-tailed Student's *t* test (Microsoft Excel).

Fluorescence images in this paper were prepared by scaling using the "autoscale" function and converting to an 8-bit pixel depth in Metamorph. FRET images were manually thresholded to mask regions where fluorescence signals were below approximately 4,000 in a range of 0 to 16,383 (14 bits) to avoid including cell-free regions where there is no fluorescence and, therefore, no FRET. FRET E_{avg} values were prepared by applying a pseudocolor map over the range of 0 to 1, as indicated on the figure color scale bars, and conversion to an 8-bit pixel depth in Metamorph. Text annotation was added using Adobe Illustrator. Images were not otherwise altered.

RESULTS

Validation of chimeric Gag constructs. To assay Gag multimerization, we created proviral molecular clones that express Gag with YFP (mVenus variant) or CFP (mCerulean variant) fused to its C terminus (Fig. 1A). To test the relative contributions of the CA-CTD and NC to Gag multimerization, we introduced deletions or point mutations (Fig. 1A). Mutations in the CA-CTD were chosen to disrupt the dimerization interface in the C-terminal domain by deleting most of the C-terminal domain (delCA-CTD) or by altering critical residues (WM184,185AA). Mutations in NC were chosen to abolish RNA binding by deleting most of the NC (delNC) or by replacing 15 basic residues with neutral residues (14A1G).

Previously, others observed that C-terminal fluorescent protein fusions to HIV-1 Gag interfere with budding of particles (55). To characterize the performance of our chimeric constructs, we performed a VLP release assay, comparing a construct expressing nonchimeric WT Gag to our chimeric constructs expressing Gag-YFP. We found that Gag-YFP is not defective in VLP release relative to that of nonchimeric Gag. However,

Gag-YFP constructs with mutations in the CA-CTD or NC were completely defective in VLP release (Fig. 1B). To confirm that our chimeric Gag species are full length, we probed parallel immunoblots with anti-p17 and anti-GFP antibodies, which recognize N and C termini, respectively (Fig. 1B). Based on the band intensities of proteins recognized by anti-GFP, greater than 97% of YFP-tagged proteins retain full-length Gag sequence.

FRET assay for Gag multimerization. When we coexpressed Gag-CFP and Gag-YFP, we detected robust FRET (Fig. 2A, bottom row, and 3B). In contrast, FRET was absent when Gag-CFP was coexpressed with cytosolic YFP (Fig. 2A, top row, and see Fig. 5B). Moreover, FRET was also absent when Gag-CFP was coexpressed with membrane-targeted Fyn(10)-YFP (Fig. 2A, middle row, and 3B). Therefore, our FRET method detected the specific interaction between Gag molecules, consistent with data from previous work (24, 45, 52, 56). The stoichiometric FRET values reported by our assay are proportional to the mole fraction of fluorescent proteins participating in FRET (41). Thus, the contributions of Gag interaction domains can be assessed quantitatively.

Consistent with previous FRET microscopy studies of Gag, the highest levels of FRET detected by our method appeared to be associated primarily with puncta on the plasma membrane (Fig. 2A, bottom row). However, moderate levels of FRET appeared diffuse throughout the cell. To more precisely localize Gag FRET within the 3D cell volume, we performed 3D epifluorescence microscopy of Gag-CFP/YFP-expressing cells immunostained without membrane permeabilization to detect plasma membrane CD81, a tetraspanin protein that colocalizes with Gag (7, 50, 68). In all cases, Gag-CFP/YFP puncta appeared on the cell surface and colocalized with CD81 immunofluorescence (Fig. 2B). To determine whether diffuse FRET throughout the cells is indicative of authentic intracellular/cytosolic Gag-Gag interactions or is a result of out-of-focus light spilling over from Gag puncta on other focal planes, we calculated FRET from 3D microscopy with or without deconvolution. Without deconvolution, FRET was calculated from single *xy* planes independently (identically to the 2D microscopy shown in Fig. 2A and throughout). As shown in Fig. 2A (bottom row), moderate levels of FRET appeared diffuse throughout the cell (Fig. 2B). However, when deconvolution was used to remove the blurred out-of-focus light from other focal planes, the FRET signals outside Gag-CFP/YFP puncta and in the cell interior were largely removed (Fig. 2B). Therefore, the moderate FRET values outside of plasma membrane puncta with 2D FRET microscopy are likely predominantly FRET signals from other focal planes, the inclusion of which is inherent to epifluorescence microscopy. Throughout this study, when FRET is quantified over multiple cells, only FRET values present at Gag puncta are included (see Materials and Methods and see Fig. S1 in the supplemental material).

To examine the effects of CA-CTD and NC mutations on Gag multimerization by FRET, we cotransfected HIV-1 molecular clones expressing CFP- and YFP-tagged WT or mutant Gag. To fully examine the phenotypes of these constructs, we tested both homotypic Gag interactions (i.e., both CFP- and YFP-tagged Gag molecules contain an identical change in the CA-CTD or NC) and heterotypic interactions between WT Gag-CFP and mutant Gag-YFP (i.e., CFP-tagged Gag molecules are WT, and YFP-tagged Gag molecules are mutant).

CA-CTD can form a "half-interface" which is only partially defective, but fully disrupting the CA-CTD dimerization interface abolishes FRET. We detected no FRET due to homotypic interactions between WM184,185AA Gag constructs or between delCA-CTD Gag constructs [not significantly different from the Fyn(10)-YFP negative control; $P > 0.01$] (Fig. 3A, second and fourth rows, and B), indicating that these mutations abolished close Gag-Gag interactions. Likewise, we detected no FRET due to heterotypic interactions between WT Gag-CFP and delCA-CTD Gag-YFP molecules [not significantly different from the Fyn(10)-YFP negative control; $P > 0.01$] (Fig. 3A, third row, and B). In these cases, the CA-CTD mutant constructs were primarily diffuse in the cytosol, suggesting that reduced membrane binding could contribute to the lack of FRET. However, some membrane lining and puncta were observed during homotypic WM184,185AA Gag-CFP/YFP expression (Fig. 3A, second row), yet these structures lacked significant FRET (Fig. 3B). We tested whether reduced membrane binding contributes to a lack of FRET by introducing mutations that directly alter membrane associations.

In contrast to the above-described experimental conditions that produced no significant Gag-Gag interaction, heterotypic interactions between WM184,185AA Gag-YFP and WT Gag-CFP produced moderately high levels of FRET, approximately 86% of that produced by the homotypic WT Gag-CFP/YFP interaction (Fig. 3A, top row, and B). As described below, this moderately high-FRET phenotype is also apparent when WT Gag-CFP was coexpressed with WM184,185AA Gag-YFP containing additional mutations [1GA and Fyn(10)] that directly alter membrane associations. As detailed in Discussion, these data suggest that the CA-CTD dimerization interface consists of two reciprocal interactions and that the disruption of one interaction still allows the formation of a half-interface.

The NC mutant is only partially defective in the context of native myristoylation. As described above, fully disrupting the CA-CTD dimerization interface produced no FRET above negative control background levels. In contrast, all experimental conditions in which NC mutants were tested produced intermediate FRET values (greater than the negative control; $P < 0.01$) (Fig. 3A and B). For both the 14A1G basic residue mutant and the NC deletion mutant, the heterotypic interaction between WT Gag-CFP and NC mutant Gag-YFP was greater than homotypic interactions between mutants ($P < 0.01$). Homotypic interactions were indistinguishable between 14A1G Gag-CFP/YFP and delNC Gag-CFP/YFP ($P > 0.01$). Altogether, these results suggest that, in contrast to CA-CTD, NC is not essential for Gag-Gag interactions as detected by FRET.

Mutations in both the CA-CTD and NC reduce steady-state Gag membrane binding. It is possible that the mutant phenotypes observed in our FRET assay are not due entirely to a primary effect of mutations on Gag-Gag interactions but rather are due partly to a secondary effect via membrane binding. This stems from the above-described findings that mutations that disrupt Gag multimerization also reduce Gag membrane binding and, conversely, that membrane binding affects Gag multimerization (see above).

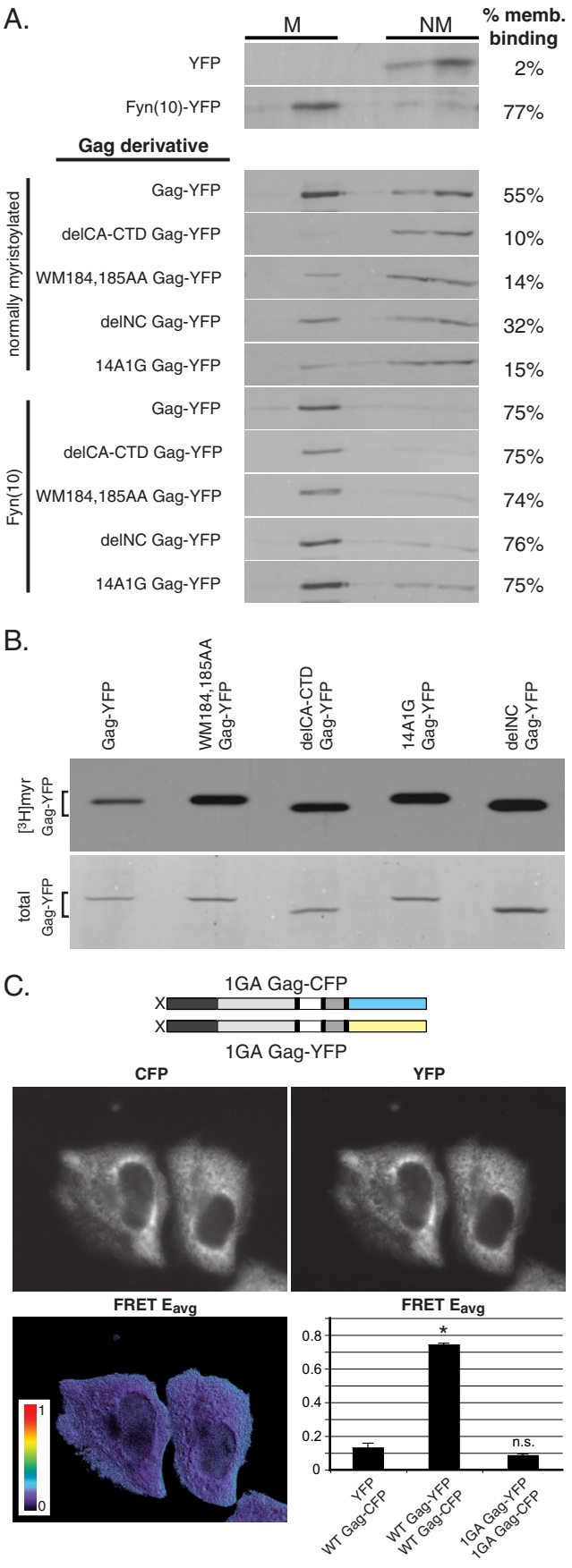

Previous studies showed that the WM184,185AA mutation reduces Gag membrane binding, whereas changes in the NC basic residues do not (74). However, these experiments examined the initial rate of membrane association of newly synthesized Gag but not the steady-state membrane binding levels that are more relevant to the interpretation of FRET microscopy data. To examine the effect of CA-CTD and NC mutations on the steady-state membrane binding of Gag-YFP, we performed a membrane flotation assay and quantified the amount of membrane-associated Gag-YFP by immunoblotting. We found that more than half of the WT Gag-YFP was membrane associated, whereas CA-CTD and NC mutations reduced membrane binding (Fig. 4A). Both CA-CTD mutations (delCA-CTD and WM184,185AA) and mutations in the basic residues of NC (14A1G) reduced membrane binding severely, whereas an NC deletion (delNC) had a less severe effect. This membrane binding defect in mutant Gag derivatives is not due to a defect in myristoylation (Fig. 4B). Because these mutations alter membrane associations to different degrees, to accurately assess the effect of these mutations on Gag-Gag interactions, it is necessary to control for this effect on membrane binding.

In the absence of myristoylation, both CA-CTD and NC mutations cause a complete loss of interactions with WT Gag molecules. To control the effect of CA-CTD and NC mutations on membrane binding and to determine how membrane binding modulates Gag multimerization, we impaired membrane binding by introducing a mutation that abolishes the N-terminal myristoylation of Gag (1GA). We detected no homotypic interaction between 1GA Gag-CFP/YFP constructs either at the plasma membrane or in the cytosol (Fig. 4C), in agreement with data from previous studies (59). In other experimental systems, Gag multimerization was detected in the absence of membrane binding (14, 61, 101). In this experimental system, in which Gag is expressed from a proviral molecular clone,

FIG. 4. (A) Membrane binding analysis of Gag derivatives. Fluorescent protein constructs [YFP and Fyn(10)-YFP] or chimeric Gag constructs (Fig. 1A) were expressed in HeLa cells and then subjected to membrane flotation centrifugation, divided into five equal-volume fractions, and detected by immunoblotting with anti-GFP. The left two fractions include membrane-associated material (M), whereas the right two fractions include non-membrane-associated material (NM). The percentage of membrane binding was calculated by the ratio of membrane-associated signal to total signal. Data are representative of data from three independent experiments in the case of normally myristoylated constructs and two independent experiments in the case of Fyn(10) constructs. (B) Gag derivatives are myristoylated. Cells expressing chimeric Gag constructs were metabolically labeled with [^{3}H]myristic acid ([^{3}H]myr) and analyzed by autoradiography to detect myristoylated Gag (top) or by immunoblotting with anti-GFP antibody to detect total Gag-YFP proteins (bottom). (C) Myristoylation of Gag is necessary to detect FRET. Myristoylation-defective (1GA) Gag-CFP/YFP constructs were coexpressed. The FRET E_{avg} values were calculated as described in the legend of Fig. 2. FRET E_{avg} values are color coded according to the scale bar. Average FRET values were quantified over 10 cells and compared with those under negative control and WT Gag-CFP/YFP conditions shown in Fig. 2 (bar graph). *, statistically greater than the YFP negative control ($P < 0.01$.); n.s., not statistically different from the YFP negative control ($P > 0.05$). Error bars represent standard errors of the means.

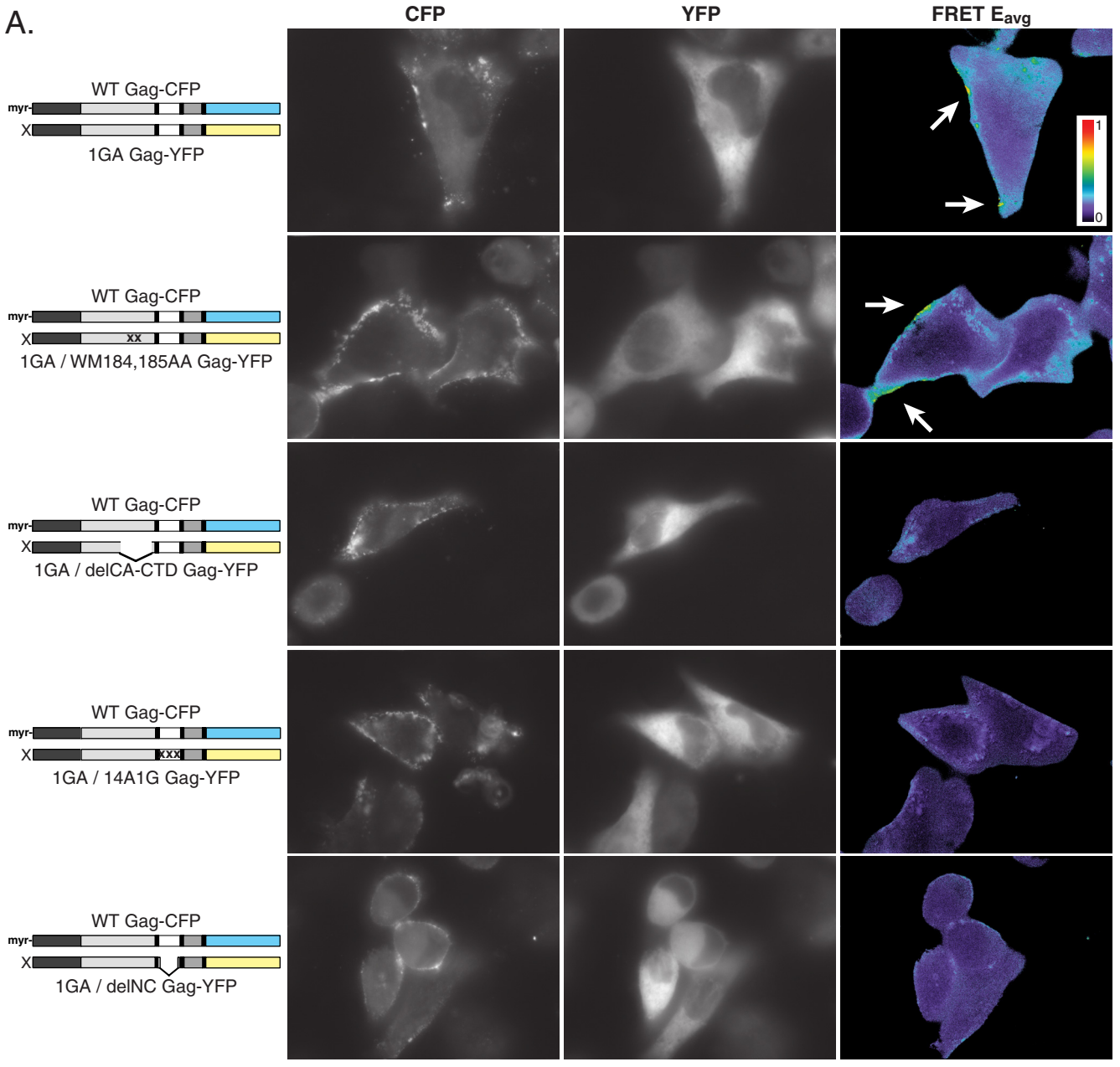
A.
CFP
YFP
FRET Eavg
WT Gag-CFP
myr-
X
1GA Gag-YFP
1
0
WT Gag-CFP
myr-
X
xx
1GA / WM184,185AA Gag-YFP
WT Gag-CFP
myr-
X
1GA / delCA-CTD Gag-YFP
WT Gag-CFP
myr-
X
xxx
1GA / 14A1G Gag-YFP
WT Gag-CFP
myr-
X
1GA / delNC Gag-YFP

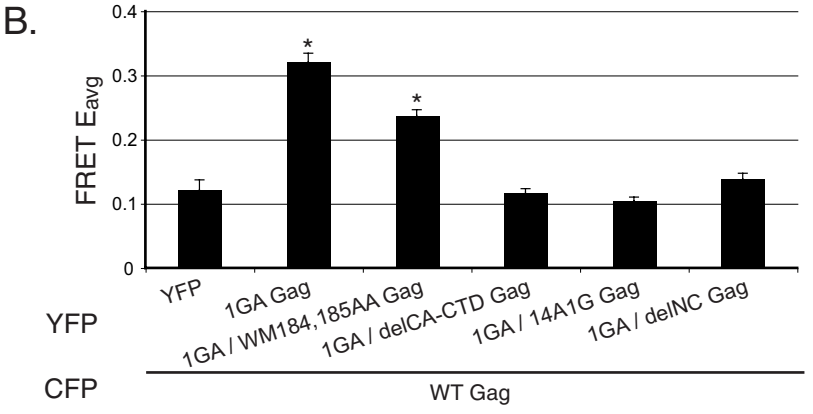
B.
FRET Eavg
0.4
0.3
0.2
0.1
0
*
*
YFP
1GA Gag
1GA / WM184,185AA Gag
1GA / delCA-CTD Gag
1GA / 14A1G Gag
1GA / delNC Gag
YFP
CFP
WT Gag

myristoylation is required for Gag-Gag interactions detected by FRET.

However, it was previously demonstrated that normally myristoylated Gag can interact with nonmyristoylated Gag and rescue it into virus particles (11, 53, 66, 70, 77), and this interaction can be detected by FRET (59). We took advantage of this observation to examine the role of the NC and CA-CTD interactions by coexpressing nonmyristoylated mutant Gag-YFP constructs with normally myristoylated WT Gag-CFP. In this system, interactions driven by the CA-CTD and NC domains can produce FRET, yet the secondary effects of CA-CTD and NC mutations via membrane binding are controlled because membrane binding is severely disrupted in the mutant constructs.

We detected FRET between WT Gag-CFP and 1GA Gag-YFP, which was associated with WT Gag-CFP plasma membrane puncta (statistically greater than the YFP negative control; $P < 0.01$) (Fig. 5A, top row, and B). Consistent with the results shown in Fig. 3, which suggest a CA-CTD "half-interface," the coexpression of WT Gag-CFP and 1GA/WM184,185AA Gag-YFP is only partially defective relative to that of WT Gag-CFP/1GA Gag-YFP (statistically greater than the YFP negative control; $P < 0.01$) (Fig. 5A, second row, and B). Also consistent with the normally myristoylated constructs shown in Fig. 3, we detected no FRET when the CA-CTD dimerization interface was fully abolished (WT Gag-CFP and 1GA/delCA-CTD Gag-YFP) (not significantly different from the YFP negative control; $P > 0.01$) (Fig. 5A, third row, and B). Notably, in contrast to results shown in Fig. 3, we detected no FRET when NC was disrupted despite the presence of an intact CA-CTD (WT Gag-CFP and either 1GA/14A1G or 1GA/delNC Gag-YFP) (not significantly different from the YFP negative control; $P > 0.01$) (Fig. 5A, fourth and bottom rows, and B). Thus, without myristoylation, NC function is necessary for Gag-Gag interactions detected by FRET. Together with the data shown in Fig. 3, these results indicate that the CA-CTD dimerization interface alone is not sufficient: either myristoylation or NC is required for mutant Gag derivatives to interact with WT Gag.

Constitutive and enhanced membrane binding can rescue the interaction of the NC mutant, but not the CA-CTD mutant, with WT Gag. As an alternative way of controlling the effect of CA-CTD and NC mutations on membrane binding and additionally to determine the effect of membrane binding on the ability of Gag mutants to multimerize, we next examined constitutively membrane binding Gag derivatives. Membrane binding was enhanced by a 10-residue exogenous triple-acylation signal derived from Fyn kinase [Fyn(10)] at their N termini. This modification was previously shown to confer cholesterol independence (73) and phosphatidylinositol-(4,5)-bisphosphate independence (17) on Gag membrane binding. We performed a membrane flotation assay on these constructs to ensure that CA-CTD and NC mutations do not have an effect on membrane binding in the context of Fyn(10). We found that the Fyn(10) triple-acylation signal causes ~75% membrane binding in all constructs regardless of a CA-CTD or NC disruption (Fig. 4A). Thus, membrane binding in the context of Fyn(10) is likely to be unaltered by the multimerization ability of these derivatives.

When we coexpressed Fyn(10)-modified CA-CTD or NC mutant Gag-YFP with WT Gag-CFP (Fig. 6), FRET results were mostly in agreement with those for normally myristoylated constructs (Fig. 3). We detected a strong interaction between WT Gag-CFP and Fyn(10) Gag-YFP (Fig. 6A, top row, and B). Consistent with the formation of a "half-interface," we detected moderately high levels of FRET between WT Gag-CFP and Fyn(10)/WM184,185AA Gag-YFP [statistically greater than the Fyn(10)-YFP negative control; $P < 0.01$] (Fig. 6A, second row, and B). However, we detected no FRET between WT Gag-CFP and Fyn(10)/delCA-CTD Gag-YFP [not significantly different from the Fyn(10)-YFP negative control; $P > 0.01$] (Fig. 6A, third row, and B). Although not directly comparable to the data from coexpression with WT Gag-CFP described above, we also tested homotypic interactions between Fyn(10)/WM184,185AA Gag-CFP/YFP and Fyn(10)/delCA-CTD Gag-CFP/YFP. We found no significant difference ($P > 0.01$) (data not shown), which is consistent with a half-interface model in that the homotypic expression of WM184,185AA mutants should be as defective as that of the delCA-CTD deletion mutant. Since CA-CTD mutant phenotypes were relatively unchanged by the addition of the Fyn(10) sequence, these results indicate that the Gag multimerization defect seen in CA-CTD mutants is a direct consequence of defective Gag-Gag interactions and not due to a secondary effect via membrane binding.

However, in contrast to results from normally myristoylated NC mutant constructs, we found near-WT levels of FRET between WT Gag-CFP and either Fyn(10)/14A1G or Fyn(10)/delNC Gag-YFP [not significantly different from WT Gag-CFP/Fyn(10) Gag-YFP; $P > 0.01$] (Fig. 6A, fourth and bottom rows, and B). These data demonstrate that constitutive or enhanced membrane binding can rescue NC mutant interactions with WT Gag-CFP multimers, suggesting functional compensation between membrane binding and NC function.

DISCUSSION

Previous studies have demonstrated the importance of the CA-CTD, NC, and membrane association during HIV-1 as-

FIG. 5. Stoichiometric FRET microscopy of N-terminal myristoylation (myr)-deficient constructs. (A) Myristoylation-defective (1GA) Gag-YFP constructs containing CA mutations (WM184,185AA or delCA-CTD) or NC mutations (14A1G or delNC) were coexpressed with WT Gag-CFP. FRET E_{avg} values were calculated as described in the legend of Fig. 2. FRET E_{avg} values are color coded according to the scale bar at the top right. Puncta with higher FRET efficiencies are indicated (arrows). (B) E_{avg} values for fluorescent puncta over approximately 50 cells were quantified and are representative of data from three independent experiments (see Fig. S1 in the supplemental material for examples of how regions of interest were selected around fluorescent puncta). Note that the impacts of CA mutations on 1GA Gag-YFP interactions with WT Gag-CFP are similar to those on Gag-YFP interactions with WT Gag-CFP (Fig. 3); however, NC mutant Gag constructs are completely defective, unlike their normally myristoylated counterparts (Fig. 3). *, statistically greater than the YFP negative control ($P < 0.01$). Error bars represent standard errors of the means.

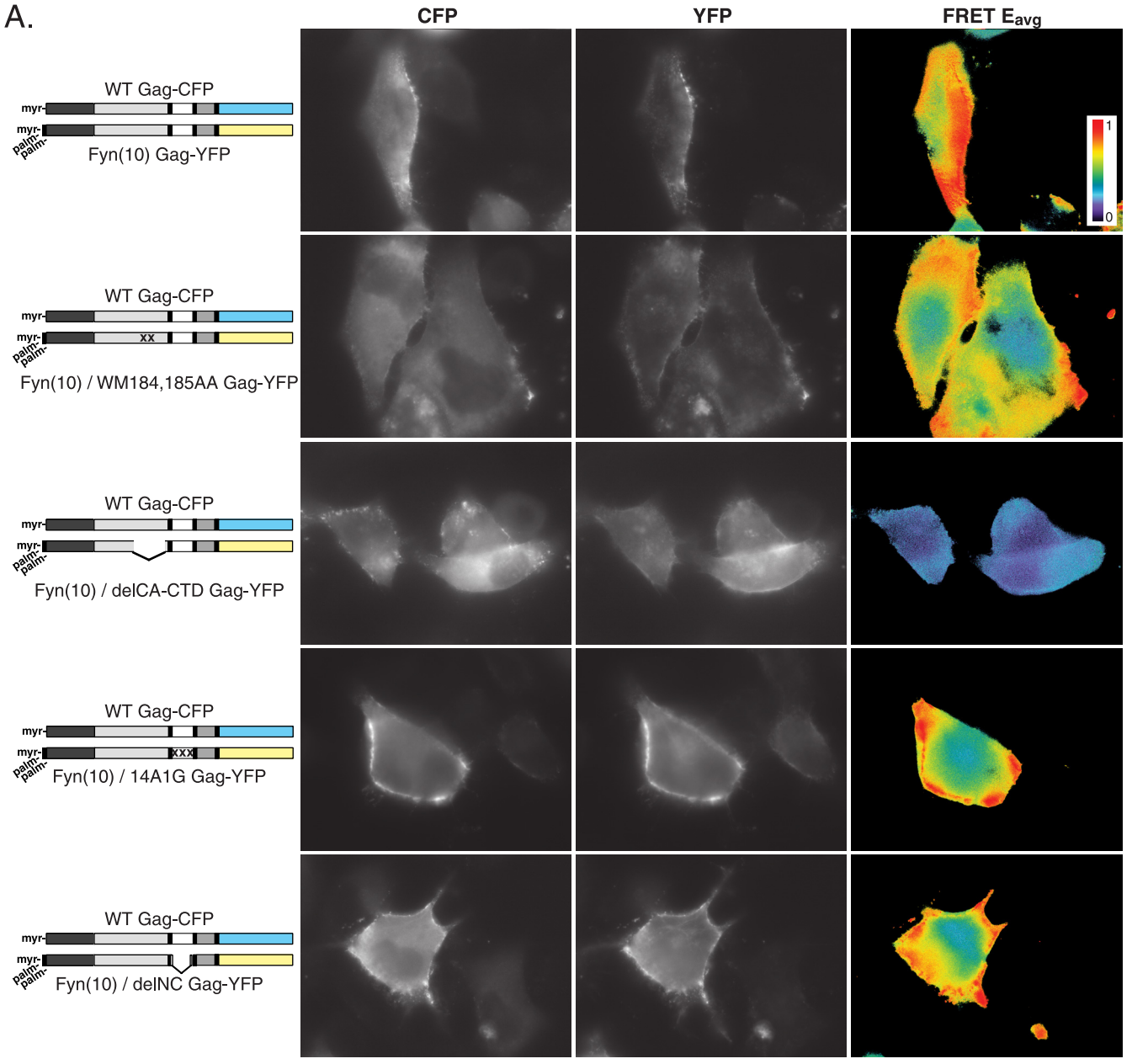
A.
CFP
YFP
FRET Eavg
WT Gag-CFP
myr-
myr-palm-palm-
Fyn(10) Gag-YFP
1
0
WT Gag-CFP
xx
Fyn(10) / WM184,185AA Gag-YFP
WT Gag-CFP
Fyn(10) / delCA-CTD Gag-YFP
WT Gag-CFP
xxx
Fyn(10) / 14A1G Gag-YFP
WT Gag-CFP
Fyn(10) / delNC Gag-YFP

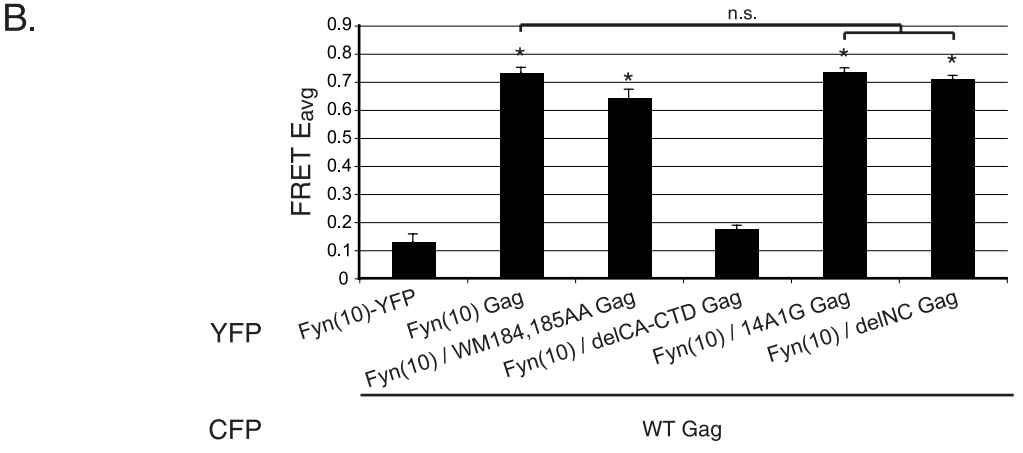
B.
n.s.
FRET Eavg
0.9
0.8
0.7
0.6
0.5
0.4
0.3
0.2
0.1
0
YFP
Fyn(10)-YFP
Fyn(10) Gag
Fyn(10) / WM184,185AA Gag
Fyn(10) / delCA-CTD Gag
Fyn(10) / 14A1G Gag
Fyn(10) / delNC Gag
CFP
WT Gag

sembly. In particular, Li et al. previously measured the multimerization of Gag derivatives by analyzing total amounts of FRET in bulk cell suspensions (59). Their study demonstrated that protein-protein interactions mediated by CA and NC-RNA interactions are important and that N-terminal myristoylation is necessary for Gag multimerization in cells (59), which our data confirmed. However, the relative contributions of and interplay between CA, NC, and membrane binding during Gag assembly in cells were not determined in previous studies. In this study, we have addressed these points by systematically altering the CA-CTD, NC, and the ability to bind membrane and by comparing the resulting Gag derivatives in a microscopy-based FRET assay.

Overall, we found that the CA-CTD is more important for close Gag-Gag interactions than is NC, as Gag with a CA-CTD deletion mutation was fully defective in all cases, whereas NC mutants were only partially defective in multimerization. In addition, our data are consistent with a model in which the CA-CTD dimerization interface consists of two reciprocal interactions, allowing the formation of a half-interface. Finally, we found that NC mutation phenotypes are affected by membrane binding, revealing functional compensation between NC function and Gag association with the membrane.

To fully test the multimerization phenotypes of Gag CA-CTD and NC mutants, we compared FRET levels in homotypic expression (i.e., FRET measured between constructs which both contain identical mutations) with those in heterotypic expression (i.e., FRET measured between WT and mutant constructs) in the context of normally myristoylated Gag (Fig. 3). The CA-CTD dimerization interface point mutant, WM184,185AA, and both NC deletion and amino acid substitution mutants showed significantly greater heterotypic interactions than homotypic interactions. This higher level of FRET due to heterotypic interactions is likely due to several causes.

First, FRET due to heterotypic interactions could be a more sensitive measure of Gag-Gag affinity, since weak interactions might be sufficient to recruit mutant Gag molecules into a multimer of WT Gag but not sufficient for mutants to form multimers alone. By this rationale, the lack of a difference between delCA-CTD homotypic and heterotypic interactions—both are completely defective—supports the importance of the CA-CTD and the relative unimportance of NC in Gag multimerization. Alternatively, greater heterotypic interactions suggest that WT molecules can provide in *trans* a function that the mutant construct lacks either to individual molecules or to the Gag multimer as a whole, such as the ability to bind membrane. In light of our finding that NC mutation phenotypes are affected by membrane binding, this is a likely explanation for the greater heterotypic interactions seen with NC mutants. This possibility is more directly addressed by the experiments in which we altered the membrane binding of mutant constructs in *cis*, as discussed below. Finally, in the case of the CA-CTD dimerization interface mutant WM184,185AA, the great difference between homotypic (WM184,185AA Gag-CFP/YFP) and heterotypic (WM184,185AA Gag-YFP coexpressed with WT Gag-CFP) interactions suggests that the CA-CTD dimerization interface is actually composed of two reciprocal interactions, one of which can be abolished to form a "half-interface." The possibility of a half-interface can be inferred from structural studies of isolated CA domain fragments: CA appears to dimerize by the burial and hydrophobic packing of critical residues W184 and M185 of one CA-CTD fragment into a mostly hydrophobic pocket on the second CA-CTD fragment (100) and vice versa. During the heterodimerization of WT and WM184,185AA mutant molecules, the WT molecule can interact with the mutant, but the mutant cannot perform the reciprocal interaction, leading to a partial interface. Others previously presented in vitro evidence for the existence of a CA-CTD "half-interface" using nonmyristoylated, truncated Gag derivatives (22). Our data provide evidence of the same phenomenon using full-length Gag derivatives in a cell-based assay and support the possibility that the Gag-Gag interface mediated by the CA-CTD is the same as or similar to the interface previously observed between isolated, mature CA proteins.

As described above, Gag membrane binding and multimerization are interrelated phenomena. An important caveat to the interpretation of CA-CTD and NC mutant phenotypes is that multimerization defects imposed by these mutations affect Gag membrane associations (Fig. 4A), which could, in turn, have a secondary effect on Gag multimerization. Therefore, we genetically separated the primary effect of mutations (i.e., the effect on protein-protein or protein-RNA scaffolding interactions) from the secondary effect on multimerization via membrane binding by altering the N-terminal acylation of Gag. By comparing CA-CTD mutation constructs to their WT counterparts under each membrane binding condition, we found the relative phenotypes of CA-CTD mutants to be consistent regardless of membrane binding changes. Therefore, we conclude that the CA-CTD mutations directly affect Gag-Gag interactions, with little or no secondary effect via a membrane binding defect. Comparing NC mutation constructs to their WT counterparts under each membrane binding condition reveals discordant results: the defect in the interaction between NC mutant and WT Gag is exacerbated by abolished mem-

FIG. 6. Stoichiometric FRET microscopy of constructs with constitutively enhanced membrane binding. (A) Gag-YFP constructs modified with a triple-acylation signal [Fyn(10)], additionally containing CA mutations (WM184,185AA or delCA-CTD) or NC mutations (14A1G or delNC), were coexpressed with WT Gag-CFP. FRET E_{avg} values were calculated as described in the legend of Fig. 2. FRET E_{avg} values are color coded according to the scale bar at the top right. myr, myristoylation; palm, palmitoylation. (B) E_{avg} values for fluorescent puncta over approximately 50 cells were quantified and are representative of data from four independent experiments (see Fig. S1 in the supplemental material for examples of how regions of interest were selected around fluorescent puncta). Note that the impacts of CA mutations on Fyn(10) Gag-YFP interactions with WT Gag-CFP are similar to those on Gag-YFP interactions with WT Gag-CFP (Fig. 3); however, NC mutant Gag constructs are rescued into WT Gag-CFP puncta at near-WT levels, unlike their normally myristoylated or myristoylation-deficient counterparts (Fig. 3 and 5). *, statistically greater than the Fyn(10)-YFP negative control ($P < 0.01$); n.s., no statistical difference ($P > 0.01$). Error bars represent standard errors of the means.

brane binding but rescued to WT levels by constitutive and enhanced membrane binding.

Previous biochemical studies have given rise to a model in which RNA serves as a scaffold for a growing Gag multimer (11, 14–16, 37, 46, 67). It has also been postulated that cellular membranes, particularly membrane microdomains, could serve as platforms for Gag multimerization (72). Our results provide evidence, using full-length Gag constructs in the biologically relevant milieu of the cell, to link these two models: the ability to bind at least one of either membrane or RNA is required for a Gag derivative with an intact CA-CTD to be rescued into multimers of WT Gag. Furthermore, our observation of functional compensation between membrane binding and NC function suggests that the two play complementary mechanistic roles, such as a scaffold, during Gag multimerization.

ACKNOWLEDGMENTS

We thank E. Freed for critical review of the manuscript. We thank M. Imperiale, J. Linderman, S. Marino, J. Swanson, A. Telesnitsky, and members of the Ono laboratory for helpful discussions; S. Straight and the University of Michigan Center for Live-Cell Imaging for fluorescence microscopy assistance; V. Boyko, W.-S. Hu, and D. Ott for reagents; and A. Lecorps, L. Goo, S. Oh, and J. Inlora for technical assistance. The following reagents were obtained through the AIDS Research and Reference Reagent Program, Division of AIDS, NIAID, NIH: HIV-Ig from NABI and NHLBI and antiserum to HIV-1 p17 from Paul Spearman.

This work was supported by NIH grant R01 AI071727 (A.O.) and NIH training grant T32 GM007544 (I.B.H.).

REFERENCES

1. **Accola, M. A., B. Strack, and H. G. Gottlinger.** 2000. Efficient particle production by minimal Gag constructs which retain the carboxy-terminal domain of human immunodeficiency virus type 1 capsid-p2 and a late assembly domain. J. Virol. **74:**5395–5402.
2. **Adachi, A., H. E. Gendelman, S. Koenig, T. Folks, R. Willey, A. Rabson, and M. A. Martin.** 1986. Production of acquired immunodeficiency syndrome-associated retrovirus in human and nonhuman cells transfected with an infectious molecular clone. J. Virol. **59:**284–291.
3. **Adamson, C. S., and I. M. Jones.** 2004. The molecular basis of HIV capsid assembly—five years of progress. Rev. Med. Virol. **14:**107–121.
4. **Alfadhli, A., T. C. Dhenub, A. Still, and E. Barklis.** 2005. Analysis of human immunodeficiency virus type 1 Gag dimerization-induced assembly. J. Virol. **79:**14498–14506.
5. **Barklis, E., J. McDermott, S. Wilkens, E. Schabtach, M. F. Schmid, S. Fuller, S. Karanjia, Z. Love, R. Jones, Y. Rui, X. Zhao, and D. Thompson.** 1997. Structural analysis of membrane-bound retrovirus capsid proteins. EMBO J. **16:**1199–1213.
6. **Beemiller, P., A. D. Hoppe, and J. A. Swanson.** 2006. A phosphatidylinositol-3-kinase-dependent signal transition regulates ARF1 and ARF6 during Fcgamma receptor-mediated phagocytosis. PLoS Biol. **4:**e162.
7. **Booth, A. M., Y. Fang, J. K. Fallon, J. M. Yang, J. E. Hildreth, and S. J. Gould.** 2006. Exosomes and HIV Gag bud from endosome-like domains of the T cell plasma membrane. J. Cell Biol. **172:**923–935.
8. **Borsetti, A., A. Ohagen, and H. G. Gottlinger.** 1998. The C-terminal half of the human immunodeficiency virus type 1 Gag precursor is sufficient for efficient particle assembly. J. Virol. **72:**9313–9317.
9. **Bowzard, J. B., R. P. Bennett, N. K. Krishna, S. M. Ernst, A. Rein, and J. W. Wills.** 1998. Importance of basic residues in the nucleocapsid sequence for retrovirus Gag assembly and complementation rescue. J. Virol. **72:**9034–9044.
10. **Bryant, M., and L. Ratner.** 1990. Myristoylation-dependent replication and assembly of human immunodeficiency virus 1. Proc. Natl. Acad. Sci. USA **87:**523–527.
11. **Burniston, M. T., A. Cimarelli, J. Colgan, S. P. Curtis, and J. Luban.** 1999. Human immunodeficiency virus type 1 Gag polyprotein multimerization requires the nucleocapsid domain and RNA and is promoted by the capsid-dimer interface and the basic region of matrix protein. J. Virol. **73:**8527–8540.
12. **Cai, D., A. D. Hoppe, J. A. Swanson, and K. J. Verhey.** 2007. Kinesin-1 structural organization and conformational changes revealed by FRET stoichiometry in live cells. J. Cell Biol. **176:**51–63.
13. **Callahan, E. M., and J. W. Wills.** 2003. Link between genome packaging and rate of budding for Rous sarcoma virus. J. Virol. **77:**9388–9398.
14. **Campbell, S., and A. Rein.** 1999. In vitro assembly properties of human immunodeficiency virus type 1 Gag protein lacking the p6 domain. J. Virol. **73:**2270–2279.
15. **Campbell, S., and V. M. Vogt.** 1997. In vitro assembly of virus-like particles with Rous sarcoma virus Gag deletion mutants: identification of the p10 domain as a morphological determinant in the formation of spherical particles. J. Virol. **71:**4425–4435.
16. **Campbell, S., and V. M. Vogt.** 1995. Self-assembly in vitro of purified CA-NC proteins from Rous sarcoma virus and human immunodeficiency virus type 1. J. Virol. **69:**6487–6497.
17. **Chukkapalli, V., I. B. Hogue, V. Boyko, W.-S. Hu, and A. Ono.** 2008. Interaction between the human immunodeficiency virus type 1 Gag matrix domain and phosphatidylinositol-(4,5)-bisphosphate is essential for efficient Gag membrane binding. J. Virol. **82:**2405–2417.
18. **Cimarelli, A., and J. Luban.** 2000. Human immunodeficiency virus type 1 virion density is not determined by nucleocapsid basic residues. J. Virol. **74:**6734–6740.
19. **Crist, R. M., S. A. Datta, A. G. Stephen, F. Soheilian, J. Mirro, R. J. Fisher, K. Nagashima, and A. Rein.** 2009. Assembly properties of human immunodeficiency virus type 1 Gag-leucine zipper chimeras: implications for retrovirus assembly. J. Virol. **83:**2216–2225.
20. **Dalton, A. K., D. Ako-Adjei, P. S. Murray, D. Murray, and V. M. Vogt.** 2007. Electrostatic interactions drive membrane association of the human immunodeficiency virus type 1 Gag MA domain. J. Virol. **81:**6434–6445.
21. **Dalton, A. K., P. S. Murray, D. Murray, and V. M. Vogt.** 2005. Biochemical characterization of Rous sarcoma virus MA protein interaction with membranes. J. Virol. **79:**6227–6238.
22. **Datta, S. A., Z. Zhao, P. K. Clark, S. Tarasov, J. N. Alexandratos, S. J. Campbell, M. Kvaratskhelia, J. Lebowitz, and A. Rein.** 2007. Interactions between HIV-1 Gag molecules in solution: an inositol phosphate-mediated switch. J. Mol. Biol. **365:**799–811.
23. **Dawson, L., and X. F. Yu.** 1998. The role of nucleocapsid of HIV-1 in virus assembly. Virology **251:**141–157.
24. **Derdowski, A., L. Ding, and P. Spearman.** 2004. A novel fluorescence resonance energy transfer assay demonstrates that the human immunodeficiency virus type 1 $Pr55^{Gag}$ I domain mediates Gag-Gag interactions. J. Virol. **78:**1230–1242.
25. **Dorfman, T., J. Luban, S. P. Goff, W. A. Haseltine, and H. G. Gottlinger.** 1993. Mapping of functionally important residues of a cysteine-histidine box in the human immunodeficiency virus type 1 nucleocapsid protein. J. Virol. **67:**6159–6169.
26. **Dussupt, V., M. P. Javid, G. Abou-Jaoude, J. A. Jadwin, J. de La Cruz, K. Nagashima, and F. Bouamr.** 2009. The nucleocapsid region of HIV-1 Gag cooperates with the PTAP and LYPXnL late domains to recruit the cellular machinery necessary for viral budding. PLoS Pathog. **5:**e1000339.
27. **Ehrlich, L. S., B. E. Agresta, and C. A. Carter.** 1992. Assembly of recombinant human immunodeficiency virus type 1 capsid protein in vitro. J. Virol. **66:**4874–4883.
28. **Feng, Y. X., T. Li, S. Campbell, and A. Rein.** 2002. Reversible binding of recombinant human immunodeficiency virus type 1 Gag protein to nucleic acids in virus-like particle assembly in vitro. J. Virol. **76:**11757–11762.
29. **Franke, E. K., H. E. Yuan, K. L. Bossolt, S. P. Goff, and J. Luban.** 1994. Specificity and sequence requirements for interactions between various retroviral Gag proteins. J. Virol. **68:**5300–5305.
30. **Freed, E. O.** 1998. HIV-1 Gag proteins: diverse functions in the virus life cycle. Virology **251:**1–15.
31. **Freed, E. O., and M. A. Martin.** 1994. Evidence for a functional interaction between the V1/V2 and C4 domains of human immunodeficiency virus type 1 envelope glycoprotein gp120. J. Virol. **68:**2503–2512.
32. **Freed, E. O., J. M. Orenstein, A. J. Buckler-White, and M. A. Martin.** 1994. Single amino acid changes in the human immunodeficiency virus type 1 matrix protein block virus particle production. J. Virol. **68:**5311–5320.
33. **Gamble, T. R., S. Yoo, F. F. Vajdos, U. K. von Schwedler, D. K. Worthylake, H. Wang, J. P. McCutcheon, W. I. Sundquist, and C. P. Hill.** 1997. Structure of the carboxyl-terminal dimerization domain of the HIV-1 capsid protein. Science **278:**849–853.
34. **Gheysen, D., E. Jacobs, F. de Foresta, C. Thiriart, M. Francotte, D. Thines, and M. De Wilde.** 1989. Assembly and release of HIV-1 precursor Pr55gag virus-like particles from recombinant baculovirus-infected insect cells. Cell **59:**103–112.
35. **Gottlinger, H. G., J. G. Sodroski, and W. A. Haseltine.** 1989. Role of capsid precursor processing and myristoylation in morphogenesis and infectivity of human immunodeficiency virus type 1. Proc. Natl. Acad. Sci. USA **86:**5781–5785.
36. **Gross, I., H. Hohenberg, C. Huckhagel, and H. G. Krausslich.** 1998. N-terminal extension of human immunodeficiency virus capsid protein converts the in vitro assembly phenotype from tubular to spherical particles. J. Virol. **72:**4798–4810.
37. **Gross, I., H. Hohenberg, and H. G. Krausslich.** 1997. In vitro assembly properties of purified bacterially expressed capsid proteins of human immunodeficiency virus. Eur. J. Biochem. **249:**592–600.
38. **Hermida-Matsumoto, L., and M. D. Resh.** 1999. Human immunodeficiency

virus type 1 protease triggers a myristoyl switch that modulates membrane binding of $Pr55^{gag}$ and p17MA. J. Virol. **73:**1902–1908.

39. **Hill, C. P., D. Worthylake, D. P. Bancroft, A. M. Christensen, and W. I. Sundquist.** 1996. Crystal structures of the trimeric human immunodeficiency virus type 1 matrix protein: implications for membrane association and assembly. Proc. Natl. Acad. Sci. USA **93:**3099–3104.
40. **Hockley, D. J., M. V. Nermut, C. Grief, J. B. Jowett, and I. M. Jones.** 1994. Comparative morphology of Gag protein structures produced by mutants of the gag gene of human immunodeficiency virus type 1. J. Gen. Virol. **75**(11)**:**2985–2997.
41. **Hoppe, A., K. Christensen, and J. A. Swanson.** 2002. Fluorescence resonance energy transfer-based stoichiometry in living cells. Biophys. J. **83:** 3652–3664.
42. **Hoppe, A. D., S. L. Shorte, J. A. Swanson, and R. Heintzmann.** 2008. Three-dimensional FRET reconstruction microscopy for analysis of dynamic molecular interactions in live cells. Biophys. J. **95:**400–418.
43. **Hoshikawa, N., A. Kojima, A. Yasuda, E. Takayashiki, S. Masuko, J. Chiba, T. Sata, and T. Kurata.** 1991. Role of the gag and pol genes of human immunodeficiency virus in the morphogenesis and maturation of retrovirus-like particles expressed by recombinant vaccinia virus: an ultrastructural study. J. Gen. Virol. **72**(10)**:**2509–2517.
44. **Huang, M., J. M. Orenstein, M. A. Martin, and E. O. Freed.** 1995. $p6^{Gag}$ is required for particle production from full-length human immunodeficiency virus type 1 molecular clones expressing protease. J. Virol. **69:**6810–6818.
45. **Hubner, W., P. Chen, A. Del Portillo, Y. Liu, R. E. Gordon, and B. K. Chen.** 2007. Sequence of human immunodeficiency virus type 1 (HIV-1) Gag localization and oligomerization monitored with live confocal imaging of a replication-competent, fluorescently tagged HIV-1. J. Virol. **81:**12596–12607.
46. **Huseby, D., R. L. Barklis, A. Alfadhli, and E. Barklis.** 2005. Assembly of human immunodeficiency virus precursor Gag proteins. J. Biol. Chem. **280:**17664–17670.
47. **Jager, S., E. Gottwein, and H. G. Krausslich.** 2007. Ubiquitination of human immunodeficiency virus type 1 Gag is highly dependent on Gag membrane association. J. Virol. **81:**9193–9201.
48. **Jares-Erijman, E. A., and T. M. Jovin.** 2003. FRET imaging. Nat. Biotechnol. **21:**1387–1395.
49. **Johnson, M. C., H. M. Scobie, Y. M. Ma, and V. M. Vogt.** 2002. Nucleic acid-independent retrovirus assembly can be driven by dimerization. J. Virol. **76:**11177–11185.
50. **Jolly, C., and Q. J. Sattentau.** 2007. Human immunodeficiency virus type 1 assembly, budding, and cell-cell spread in T cells take place in tetraspanin-enriched plasma membrane domains. J. Virol. **81:**7873–7884.
51. **Joshi, A., K. Nagashima, and E. O. Freed.** 2006. Mutation of dileucine-like motifs in the human immunodeficiency virus type 1 capsid disrupts virus assembly, Gag-Gag interactions, Gag-membrane binding, and virion maturation. J. Virol. **80:**7939–7951.
52. **Jouvenet, N., P. D. Bieniasz, and S. M. Simon.** 2008. Imaging the biogenesis of individual HIV-1 virions in live cells. Nature **454:**236–240.
53. **Kawada, S., T. Goto, H. Haraguchi, A. Ono, and Y. Morikawa.** 2008. Dominant negative inhibition of human immunodeficiency virus particle production by the nonmyristoylated form of Gag. J. Virol. **82:**4384–4399.
54. **Khorchid, A., R. Halwani, M. A. Wainberg, and L. Kleiman.** 2002. Role of RNA in facilitating Gag/Gag-Pol interaction. J. Virol. **76:**4131–4137.
55. **Larson, D. R., M. C. Johnson, W. W. Webb, and V. M. Vogt.** 2005. Visualization of retrovirus budding with correlated light and electron microscopy. Proc. Natl. Acad. Sci. USA **102:**15453–15458.
56. **Larson, D. R., Y. M. Ma, V. M. Vogt, and W. W. Webb.** 2003. Direct measurement of Gag-Gag interaction during retrovirus assembly with FRET and fluorescence correlation spectroscopy. J. Cell Biol. **162:**1233–1244.
57. **Lee, E.-G., and M. L. Linial.** 2004. Basic residues of the retroviral nucleocapsid play different roles in Gag-Gag and Gag-Ψ RNA interactions. J. Virol. **78:**8486–8495.
58. **Lee, Y. M., B. Liu, and X. F. Yu.** 1999. Formation of virus assembly intermediate complexes in the cytoplasm by wild-type and assembly-defective mutant human immunodeficiency virus type 1 and their association with membranes. J. Virol. **73:**5654–5662.
59. **Li, H., J. Dou, L. Ding, and P. Spearman.** 2007. Myristoylation is required for human immunodeficiency virus type 1 Gag-Gag multimerization in mammalian cells. J. Virol. **81:**12899–12910.
60. **Lingappa, J. R., J. E. Dooher, M. A. Newman, P. K. Kiser, and K. C. Klein.** 2006. Basic residues in the nucleocapsid domain of Gag are required for interaction of HIV-1 gag with ABCE1 (HP68), a cellular protein important for HIV-1 capsid assembly. J. Biol. Chem. **281:**3773–3784.
61. **Lingappa, J. R., R. L. Hill, M. L. Wong, and R. S. Hegde.** 1997. A multistep, ATP-dependent pathway for assembly of human immunodeficiency virus capsids in a cell-free system. J. Cell Biol. **136:**567–581.
62. **Ma, Y. M., and V. M. Vogt.** 2004. Nucleic acid binding-induced Gag dimerization in the assembly of Rous sarcoma virus particles in vitro. J. Virol. **78:**52–60.
63. **Ma, Y. M., and V. M. Vogt.** 2002. Rous sarcoma virus Gag protein-oligonucleotide interaction suggests a critical role for protein dimer formation in assembly. J. Virol. **76:**5452–5462.
64. **Momany, C., L. C. Kovari, A. J. Prongay, W. Keller, R. K. Gitti, B. M. Lee, A. E. Gorbalenya, L. Tong, J. McClure, L. S. Ehrlich, M. F. Summers, C. Carter, and M. G. Rossmann.** 1996. Crystal structure of dimeric HIV-1 capsid protein. Nat. Struct. Biol. **3:**763–770.
65. **Morikawa, Y., T. Goto, and F. Momose.** 2004. Human immunodeficiency virus type 1 Gag assembly through assembly intermediates. J. Biol. Chem. **279:**31964–31972.
66. **Morikawa, Y., S. Hinata, H. Tomoda, T. Goto, M. Nakai, C. Aizawa, H. Tanaka, and S. Omura.** 1996. Complete inhibition of human immunodeficiency virus Gag myristoylation is necessary for inhibition of particle budding. J. Biol. Chem. **271:**2868–2873.
67. **Muriaux, D., J. Mirro, D. Harvin, and A. Rein.** 2001. RNA is a structural element in retrovirus particles. Proc. Natl. Acad. Sci. USA **98:**5246–5251.
68. **Nydegger, S., S. Khurana, D. N. Krementsov, M. Foti, and M. Thali.** 2006. Mapping of tetraspanin-enriched microdomains that can function as gateways for HIV-1. J. Cell Biol. **173:**795–807.
69. **Ono, A., S. D. Ablan, S. J. Lockett, K. Nagashima, and E. O. Freed.** 2004. Phosphatidylinositol (4,5) bisphosphate regulates HIV-1 Gag targeting to the plasma membrane. Proc. Natl. Acad. Sci. USA **101:**14889–14894.
70. **Ono, A., D. Demirov, and E. O. Freed.** 2000. Relationship between human immunodeficiency virus type 1 Gag multimerization and membrane binding. J. Virol. **74:**5142–5150.
71. **Ono, A., and E. O. Freed.** 1999. Binding of human immunodeficiency virus type 1 Gag to membrane: role of the matrix amino terminus. J. Virol. **73:**4136–4144.
72. **Ono, A., and E. O. Freed.** 2005. Role of lipid rafts in virus replication. Adv. Virus Res. **64:**311–358.
73. **Ono, A., A. A. Waheed, and E. O. Freed.** 2007. Depletion of cellular cholesterol inhibits membrane binding and higher-order multimerization of human immunodeficiency virus type 1 Gag. Virology **360:**27–35.
74. **Ono, A., A. A. Waheed, A. Joshi, and E. O. Freed.** 2005. Association of human immunodeficiency virus type 1 Gag with membrane does not require highly basic sequences in the nucleocapsid: use of a novel Gag multimerization assay. J. Virol. **79:**14131–14140.
75. **Ott, D. E., L. V. Coren, E. N. Chertova, T. D. Gagliardi, K. Nagashima, R. C. Sowder II, D. T. Poon, and R. J. Gorelick.** 2003. Elimination of protease activity restores efficient virion production to a human immunodeficiency virus type 1 nucleocapsid deletion mutant. J. Virol. **77:**5547–5556.
76. **Paillart, J.-C., and H. G. Göttlinger.** 1999. Opposing effects of human immunodeficiency virus type 1 matrix mutations support a myristyl switch model of Gag membrane targeting. J. Virol. **73:**2604–2612.
77. **Park, J., and C. D. Morrow.** 1992. The nonmyristylated $Pr160^{gag\text{-}pol}$ polyprotein of human immunodeficiency virus type 1 interacts with $Pr55^{gag}$ and is incorporated into viruslike particles. J. Virol. **66:**6304–6313.
78. **Perez-Caballero, D., T. Hatziioannou, J. Martin-Serrano, and P. D. Bieniasz.** 2004. Human immunodeficiency virus type 1 matrix inhibits and confers cooperativity on Gag precursor-membrane interactions. J. Virol. **78:** 9560–9563.
79. **Poon, D. T., J. Wu, and A. Aldovini.** 1996. Charged amino acid residues of human immunodeficiency virus type 1 nucleocapsid p7 protein involved in RNA packaging and infectivity. J. Virol. **70:**6607–6616.
80. **Popov, S., E. Popova, M. Inoue, and H. G. Gottlinger.** 2008. Human immunodeficiency virus type 1 Gag engages the Bro1 domain of ALIX/AIP1 through the nucleocapsid. J. Virol. **82:**1389–1398.
81. **Prodanov, D., J. Heeroma, and E. Marani.** 2006. Automatic morphometry of synaptic boutons of cultured cells using granulometric analysis of digital images. J. Neurosci. Methods **151:**168–177.
82. **Provitera, P., A. Goff, A. Harenberg, F. Bouamr, C. Carter, and S. Scarlata.** 2001. Role of the major homology region in assembly of HIV-1 Gag. Biochemistry **40:**5565–5572.
83. **Resh, M. D.** 2004. A myristoyl switch regulates membrane binding of HIV-1 Gag. Proc. Natl. Acad. Sci. USA **101:**417–418.
84. **Rizzo, M. A., G. H. Springer, B. Granada, and D. W. Piston.** 2004. An improved cyan fluorescent protein variant useful for FRET. Nat. Biotechnol. **22:**445–449.
85. **Roldan, A., R. S. Russell, B. Marchand, M. Gotte, C. Liang, and M. A. Wainberg.** 2004. In vitro identification and characterization of an early complex linking HIV-1 genomic RNA recognition and Pr55Gag multimerization. J. Biol. Chem. **279:**39886–39894.
86. **Saad, J. S., E. Loeliger, P. Luncsford, M. Liriano, J. Tai, A. Kim, J. Miller, A. Joshi, E. O. Freed, and M. F. Summers.** 2007. Point mutations in the HIV-1 matrix protein turn off the myristyl switch. J. Mol. Biol. **366:**574–585.
87. **Saad, J. S., J. Miller, J. Tai, A. Kim, R. H. Ghanam, and M. F. Summers.** 2006. Structural basis for targeting HIV-1 Gag proteins to the plasma membrane for virus assembly. Proc. Natl. Acad. Sci. USA **103:**11364–11369.
88. **Sandefur, S., R. M. Smith, V. Varthakavi, and P. Spearman.** 2000. Mapping and characterization of the N-terminal I domain of human immunodeficiency virus type 1 $Pr55^{Gag}$. J. Virol. **74:**7238–7249.
89. **Sandefur, S., V. Varthakavi, and P. Spearman.** 1998. The I domain is

required for efficient plasma membrane binding of human immunodeficiency virus type 1 $Pr55^{Gag}$. J. Virol. **72:**2723–2732.
90. **Sekar, R. B., and A. Periasamy.** 2003. Fluorescence resonance energy transfer (FRET) microscopy imaging of live cell protein localizations. J. Cell Biol. **160:**629–633.
91. **Shkriabai, N., S. A. Datta, Z. Zhao, S. Hess, A. Rein, and M. Kvaratskhelia.** 2006. Interactions of HIV-1 Gag with assembly cofactors. Biochemistry **45:**4077–4083.
92. **Spearman, P., R. Horton, L. Ratner, and I. Kuli-Zade.** 1997. Membrane binding of human immunodeficiency virus type 1 matrix protein in vivo supports a conformational myristyl switch mechanism. J. Virol. **71:**6582–6592.
93. **Sutton, R. E., H. T. Wu, R. Rigg, E. Bohnlein, and P. O. Brown.** 1998. Human immunodeficiency virus type 1 vectors efficiently transduce human hematopoietic stem cells. J. Virol. **72:**5781–5788.
94. **Swanstrom, R., and J. W. Wills.** 1997. Synthesis, assembly, and processing of viral proteins, p. 263–334. *In* J. M. Coffin, S. H. Hughes, and H. E. Varmus (ed.), Retroviruses. Cold Spring Harbor Laboratory Press, Cold Spring Harbor, NY.
95. **Tang, C., E. Loeliger, P. Luncsford, I. Kinde, D. Beckett, and M. F. Summers.** 2004. Entropic switch regulates myristate exposure in the HIV-1 matrix protein. Proc. Natl. Acad. Sci. USA **101:**517–522.
96. **von Schwedler, U. K., K. M. Stray, J. E. Garrus, and W. I. Sundquist.** 2003. Functional surfaces of the human immunodeficiency virus type 1 capsid protein. J. Virol. **77:**5439–5450.
97. **Wang, C.-T., H.-Y. Lai, and J.-J. Li.** 1998. Analysis of minimal human immunodeficiency virus type 1 *gag* coding sequences capable of virus-like particle assembly and release. J. Virol. **72:**7950–7959.
98. **Wang, S. W., and A. Aldovini.** 2002. RNA incorporation is critical for retroviral particle integrity after cell membrane assembly of Gag complexes. J. Virol. **76:**11853–11865.
99. **Wang, S. W., K. Noonan, and A. Aldovini.** 2004. Nucleocapsid-RNA interactions are essential to structural stability but not to assembly of retroviruses. J. Virol. **78:**716–723.
100. **Worthylake, D. K., H. Wang, S. Yoo, W. I. Sundquist, and C. P. Hill.** 1999. Structures of the HIV-1 capsid protein dimerization domain at 2.6 Å resolution. Acta Crystallogr. D Biol. Crystallogr. **55:**85–92.
101. **Yu, F., S. M. Joshi, Y. M. Ma, R. L. Kingston, M. N. Simon, and V. M. Vogt.** 2001. Characterization of Rous sarcoma virus Gag particles assembled in vitro. J. Virol. **75:**2753–2764.
102. **Zabransky, A., E. Hunter, and M. Sakalian.** 2002. Identification of a minimal HIV-1 gag domain sufficient for self-association. Virology **294:**141–150.
103. **Zhang, W. H., D. J. Hockley, M. V. Nermut, Y. Morikawa, and I. M. Jones.** 1996. Gag-Gag interactions in the C-terminal domain of human immunodeficiency virus type 1 p24 capsid antigen are essential for Gag particle assembly. J. Gen. Virol. **77**(4)**:**743–751.
104. **Zhang, Y., and E. Barklis.** 1997. Effects of nucleocapsid mutations on human immunodeficiency virus assembly and RNA encapsidation. J. Virol. **71:**6765–6776.
105. **Zhang, Y., H. Qian, Z. Love, and E. Barklis.** 1998. Analysis of the assembly function of the human immunodeficiency virus type 1 Gag protein nucleocapsid domain. J. Virol. **72:**1782–1789.
106. **Zhou, W., L. J. Parent, J. W. Wills, and M. D. Resh.** 1994. Identification of a membrane-binding domain within the amino-terminal region of human immunodeficiency virus type 1 Gag protein which interacts with acidic phospholipids. J. Virol. **68:**2556–2569.
107. **Zhou, W., and M. D. Resh.** 1996. Differential membrane binding of the human immunodeficiency virus type 1 matrix protein. J. Virol. **70:**8540–8548.